RZ 3917 (# ZUR1705-042) 05/13/2017
Physical Sciences 30 pages

Research Report

Generation and Characterization of a *meta*-Aryne on Cu and NaCl Surfaces

Niko Pavliček,[1] Zsolt Majzik,[1] Sara Collazos,[2,3] Gerhard Meyer,[1] Dolores Pérez,[2] Enrique Guitián,[2] Diego Peña,[2] and Leo Gross[1]

[1]IBM Research–Zurich, Säumerstrasse 4, 8803 Rüschlikon, Switzerland
[2]CIQUS, Universidade de Santiago de Compostela, 15782 Santiago de Compostela, Spain
[3]Present address: AMSlab, 27003 Lugo, Spain

Generation and Characterization of a *meta*-Aryne on Cu and NaCl Surfaces

Niko Pavliček,[†] Zsolt Majzik,[†] Sara Collazos,[‡,¶] Gerhard Meyer,[†] Dolores Pérez,[‡] Enrique Guitián,[‡] Diego Peña,[*,‡] and Leo Gross[*,†]

[†]*IBM Research–Zurich, Säumerstrasse 4, 8803 Rüschlikon, Switzerland*

[‡]*CIQUS, Universidade de Santiago de Compostela, 15782 Santiago de Compostela, Spain*

[¶]*Present address: AMSlab, 27003 Lugo, Spain*

E-mail: diego.pena@usc.es; lgr@zurich.ibm.com

Abstract

We describe the generation of a *meta*-aryne at low temperature ($T = 5\,\mathrm{K}$) using atomic manipulation on Cu(111) and on bilayer NaCl on Cu(111). We observe different voltage thresholds for dehalogenation of the precursor and different reaction products depending on the substrate surface. The chemical structure is resolved by AFM with CO-terminated tips revealing the radical positions and confirming a diradical rather than an anti-Bredt olefin structure for this *meta*-aryne on NaCl.

Keywords

STM, AFM, atomic manipulation, aryne, reactive intermediate.

Arynes are important reactive intermediates in chemical synthesis which have been recently generated on-surface from the corresponding dihalogenated aromatic precursors by cleavage of two C-X bonds (X = Br, I).[1–7] In general, aromatic hydrocarbons substituted with halogens (Br or I) in respective positions of a benzene ring serve as molecular precursors of arynes. The carbon-halogen bonds act as predetermined breaking points that can be cleaved by means of atomic manipulation.

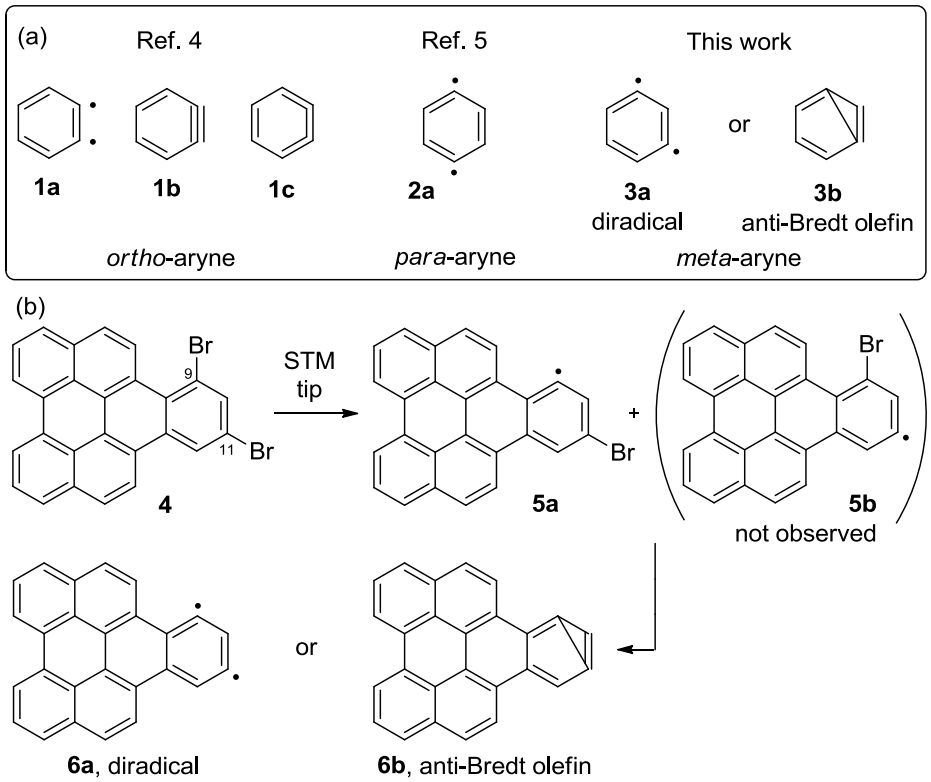

Scheme 1: (a) *ortho*-, *para*-, and *meta*-Arynes investigated in Ref. 4, Ref. 5, and this work, respectively. (b) Atomic manipulation procedure applied on **4** to generate *meta*-aryne **6**.

It has been shown that generation of arynes from physisorbed diiodobenzene (DIB) precursor molecules adsorbed on metal surfaces leads to bond formation to the metal (chemisorption).[1–3,6–8] Upon electronic excitation by tunneling electrons, C-I bonds break one-at-a-time for *para*-DIB,[1] but a single electron induces cleavage of both C-I bonds in *ortho*-DIB.[2] This difference can be rationalized by the spatial extent of the anti-bonding orbital that is temporarily occupied upon electron tunneling. Depending on the initial adsorption geometry,

both pathways are possible for *meta*-DIB.[6,7] Alternatively to electronic excitation, cleavage of the C-I bonds can be triggered by vibrational excitation.[3]

In contrast to above mentioned results on metal surfaces, both *ortho*- (**1**, Ref.[4]) and *para*-arynes (**2**, Ref.[5]) are stabilized on insulating surfaces (Scheme 1). Combined with the capability of AFM to resolve the chemical structure of individual molecules,[9] in particular intermediates and products of on-surface reactions,[10–14] this finding provides an ideal toolbox to address questions about the structure of reactive intermediates. For example, experimental AFM data in combination with density functional theory (DFT) calculations concluded a dominant cumulenic character (**1c**) for the *ortho*-aryne studied in Ref.[4]

There are controversial reports about the structure of *meta*-arynes, most of them conclude a diradical character **3a** (Scheme 1)[15–21] while a few point to the possibility of an anti-Bredt olefin structure **3b**.[22–24] A few years after first isolation of *meta*-aryne **3**,[15] DFT calculations by Hess Jr.[22,23] claimed a closed-shell structure **3b** (anti-Bredt olefin). Both theoretical studies by Kraka *et al.*[17] and Winkler and Sander[18] using the coupled cluster approach with single and double excitations and a perturbative treatment of triple excitations [CCSD(T)] and a subsequent experimental study by Sander *et al.*[19] by infrared spectroscopy in low-temperature matrices concluded a diradical structure **3a**. Also a work by Al-Saidi and Umrigar[21] using a diffusion Monte Carlo method confirmed diradical structure **3a**. However, a recent work by de Oteyza *et al.*,[24] substantiated on DFT calculations, concluded an anti-Bredt olefin structure **3b** on a Au(111) surface.

Individual molecules of **6** were generated by atomic manipulation of precursor **4** adsorbed on Cu(111) (denoted as Cu) surfaces or two-monolayer thick islands of NaCl grown on Cu(111) (denoted as NaCl). Herein, we study the *meta*-aryne model compound **6** adsorbed on the relatively inert NaCl surface and on a more reactice Cu(111) surface by high-resolution AFM. On NaCl, the *meta*-aryne revealed the diradical structure **6a**, whereas on Cu(111) the aryne formed covalent bonds towards the metal substrate.

Based on our previous experience on the on-surface generation and imaging of an *ortho*-

aryne,[4] we decided to prepare 9,11-dibromonaphtho[1,2,3,4-*ghi*]perylene (**4**) as precursor of aryne **6**. This structure was chosen deliberately because it allows direct comparison to the related *ortho*-aryne from Ref. 4 and the large polycyclic system of **6** renders a bond-order analysis possible.[25] Compound **4** was synthesized in one step by reaction of perylene with 3,5-dibromobenzyne (Supporting Information).

Results and discussion

Precursor

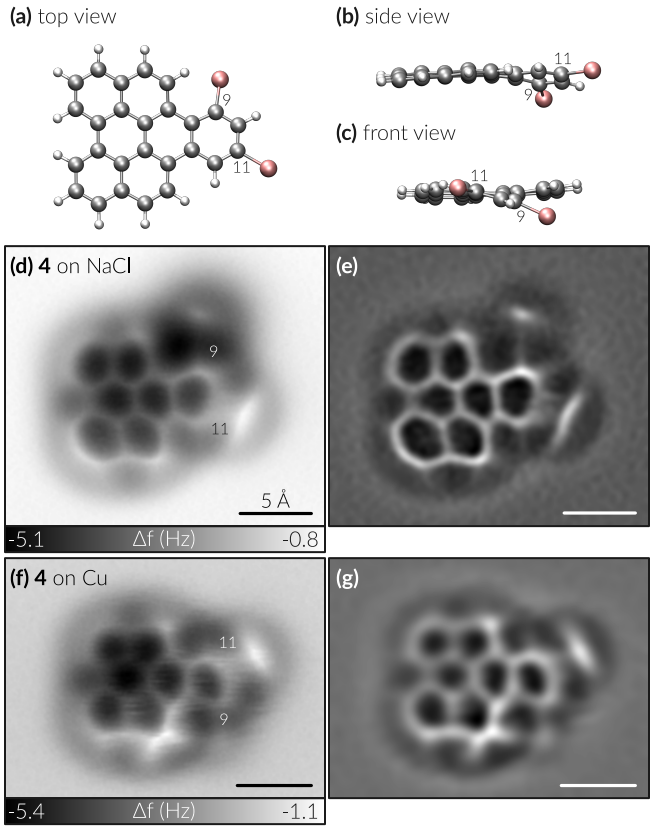

Figure 1: Characterization of precursor **4**. (a-c) Ball-and-stick models of its DFT-calculated structure seen from the top, the side, and the front, respectively. C-9 and C-11 are indicated. C, H, and Br are drawn in grey, white, and red, respectively. (d) and (f) Constant-height AFM images of **4** on NaCl ($\Delta z = 180\,\mathrm{pm}$) and Cu ($\Delta z = -120\,\mathrm{pm}$), respectively. (e) and (g) Corresponding Laplace-filtered versions to highlight the molecular structure. Note that the molecule on Cu is adsorbed with the other face to the surface. Reference set point of Δz: $I_{\mathrm{sp}} = 1\,\mathrm{pA}$, $V_{\mathrm{sp}} = 0.1\,\mathrm{V}$.

Ball-and-stick models of **4** are shown in Figs. 1a-c illustrating its non-planar geometry caused by steric hindrance of the Br atom attached to C-9 in a bay region of the molecule. This geometry is well resembled in the corresponding AFM image and its Laplace-filtered version of **4** on NaCl presented in Figs. 1d and 1e, respectively (an alternative adsorption geometry is shown in the Supporting Information). In particular, the brighter appearance of the Br connected to C-11 shows that it is closer to the tip than the one connected to C-9 (appearing less bright). Additionally, the slight increase in contrast from top to bottom of the AFM image indicates a slight tilt across the longitudinal axis. AFM data of **4** adsorbed on Cu (Figs. 1f and 1g) show even more pronounced contrast differences between the two Br atoms, and strong distortions at the bay region close to C-9. Note that the molecule shown on Cu (Figs. 1f,g) is flipped with respect to the one shown on NaCl (Figs. 1d,e). We emphasize that the distortions are expected due to tilting of the CO at the tip apex which is sensitive to non-planar adsorption geometries.[26,27]

Atomic manipulation

Atomic manipulation was previously used to cleave the respective weakest bond within a molecule.[4,5,28–32] Here, we apply this method to dissociate the Br atoms from **4**. On NaCl, the threshold voltage for dissociation was $V_{\mathrm{NaCl}} \geq 1.8\,\mathrm{V}$. This value is significantly smaller than the bond dissociation energy of about 3.6 eV (Ref. 33) but the value corresponds to the onset of the LUMO (see supplementary information), suggesting that the reaction is related to electron attachment by temporarily adding an electron to the LUMO of **4**.[4,29] Usually, a single pulse resulted in the detachment of both Br atoms. Fig. 2a-c presents a typical example of this atomic manipulation procedure. In that case the two cleaved Br atoms appear with a different contrast.[34] Upon growth of NaCl islands, the confined two-dimensional electron gas due to the surface state of Cu(111) survives at the interface of Cu and NaCl. A charged adsorbate acts as a scattering centre for the interface state electrons due to its long-range electrostatic potential.[35] Because a standing wave pattern is centered

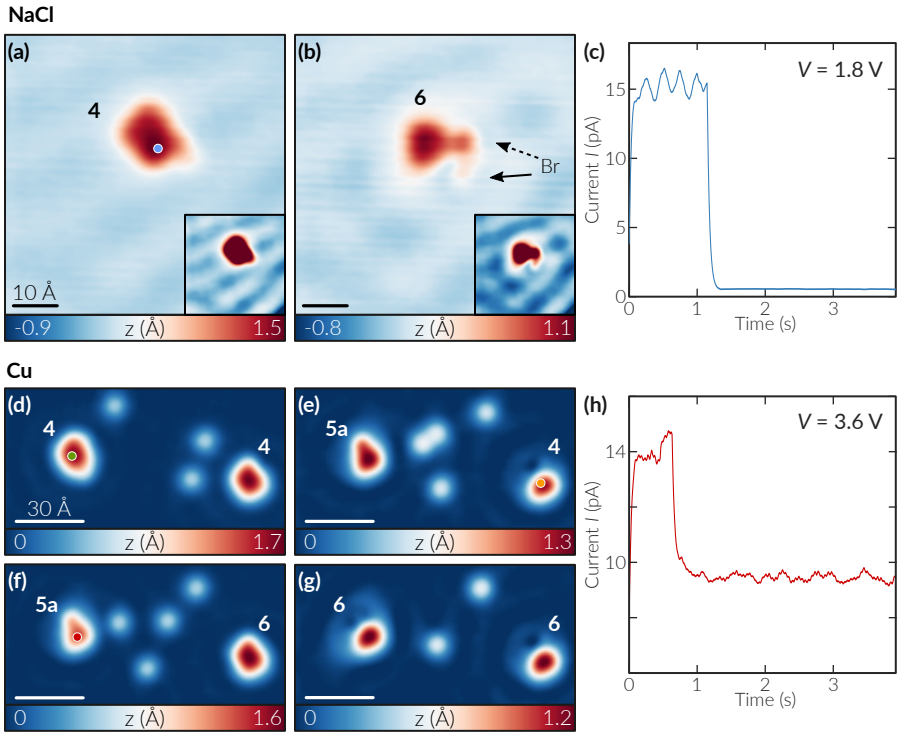

Figure 2: Atomic manipulation of precursor **4** to form **6**. (a,b) STM images of **4** before and **6** after atomic manipulation on NaCl, respectively. (c,h) Current-time traces of manipulation procedures applied at positions indicated by blue (on NaCl) and red (on Cu) circles in (a) and (f), respectively. The voltage applied during the pulse is indicated in the top right of each panel. (d-g) STM images of manipulation sequence of two precursor molecules **4** adsorbed on Cu. The first (green circle) and second (orange) pulses cleaved one and two C-Br bond of the respective molecules below the tip. The final pulse (red) cleaved the remaining C-Br bond of this molecule. The small bright features are individual Br atoms [the 3 ones in panel (d) stem from other precursor molecules, and several move out of the frame due to the high voltage applied during manipulation]. Imaging parameters: $I = 1\,\mathrm{pA}$, $V = 0.1\,\mathrm{V}$, except for panel (d), where $V = 0.2\,\mathrm{V}$.

around one of the detached Br atoms (marked by solid arrow), we conclude that this Br atom is charged, while the other (dashed arrow) is neutral. This manipulation procedure often leads to nonlocal detachment of a single Br from other, previously untouched, molecules on NaCl in a similar manner as observed for *para*-dibromo derivatives (i. e. precursors of *para*-arynes **2**).[5] For the nonlocal detachment of a single Br atom from **4** we have exclusively found structure **5a** as the product, that is the Br connected to the more steric demanding C-9 got detached. While a detailed analysis of the nonlocality is out of the scope of this paper, we speculate that it is mediated by the NaCl/Cu(111) interface state electrons.[36,37]

On Cu we observed several differences for the debromination of **4** compared to NaCl. On, Cu the threshold voltage to cleave C-Br bonds was $V_{\mathrm{Cu}} \approx 3.6\,\mathrm{V}$ corresponding to their bond dissociation energy.[33] In contrast to NaCl, bond cleavage was confined to the molecule below the tip. This finding and the significantly greater threshold for C-Br bond cleavage on Cu compared to NaCl indicate different dissociation mechanisms for the respective surfaces. We conclude that the voltage threshold on NaCl is lower than on Cu because resonant tunneling into the LUMO is dominant on the insulator, in particular facilitating vibrational excitations within the molecule. This is not a surface catalytic effect. But it demonstrates that energy barriers for reactions might be lowered by accessing ionic states of molecules on insulating substrates.[38]

Similar to the case of *meta*-DIB on Cu(110),[6,7] we have observed two possibilities: C-Br bonds break either one-at-a-time with **5a** as an intermediate or both C-Br bonds with a single voltage pulse. An example of the former is illustrated by manipulation of the molecule on the left-hand side in Fig. 2d to Fig. 2e. A subsequent manipulation step performed on the molecule on the right-hand side between Fig. 2e and Fig. 2f demonstrates an example of cleavage of both C-Br bonds with a single pulse. Finally, a successive manipulation step is used to cleave the remaining Br atom from the molecule on the left-hand side (Fig. 2f to Fig. 2g). As on NaCl, we have never observed **5b** as an intermediate on Cu.

Characterization of reaction products

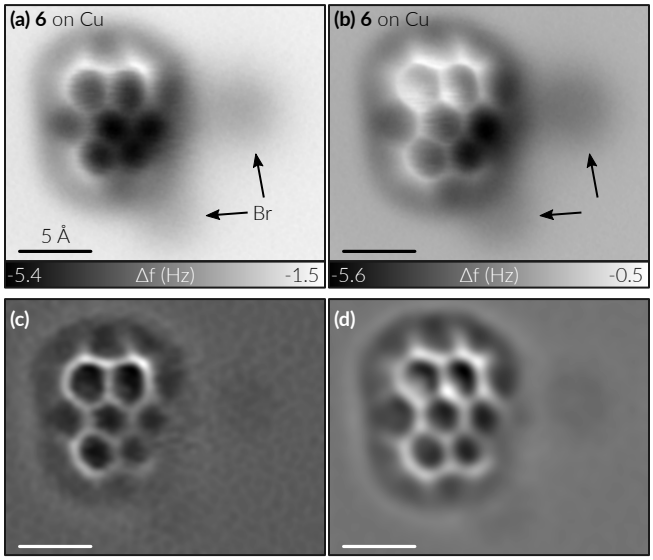

Figure 3: Visualization of aryne **6** on Cu. (a,b) AFM images of **6** at far ($\Delta z = -120\,\mathrm{pm}$) and close ($\Delta z = -150\,\mathrm{pm}$) distance, respectively. (c) and (d) show Laplace-filtered versions of (a) and (b), respectively. Cleaved Br atoms are indicated by arrows in the AFM images. Reference set point of Δz is $I_{\mathrm{sp}} = 1\,\mathrm{pA}$, $V_{\mathrm{sp}} = 0.1\,\mathrm{V}$.

Next, we discuss the behaviour of this *meta*-aryne created by atom manipulation on the Cu surface. After breaking both C-Br bonds of a precursor **4** by a single manipulation event, the AFM images presented in Fig. 3 reveal drastic changes of the molecular structure (compared to AFM data of **4** in Fig. 1f and 1g discussed above). The contrast is explained by covalent bonds formed between the aryne **6** and the Cu(111) surface.[1–7] Because the aryne-related part tilts towards the surface, it is not visible in the AFM images.[4,5] The detached Br atoms, indicated by blue arrows, show up as faint features of more negative frequency shift Δf. For the structure **6a** such chemisorption is expected as other σ radicals showed chemisorption with a bent adsorption geometry due to covalent bonds formed to the metal surface.[4,5,39] In contrast for the π radical triangulene a planar adsorption geometry was observed on the Cu(111) surface.[31]

By contrast, the generation of the *meta*-aryne on NaCl resulted in a planar product. This allowed us to characterize the outermost six-membered ring with the aryne moiety, providing

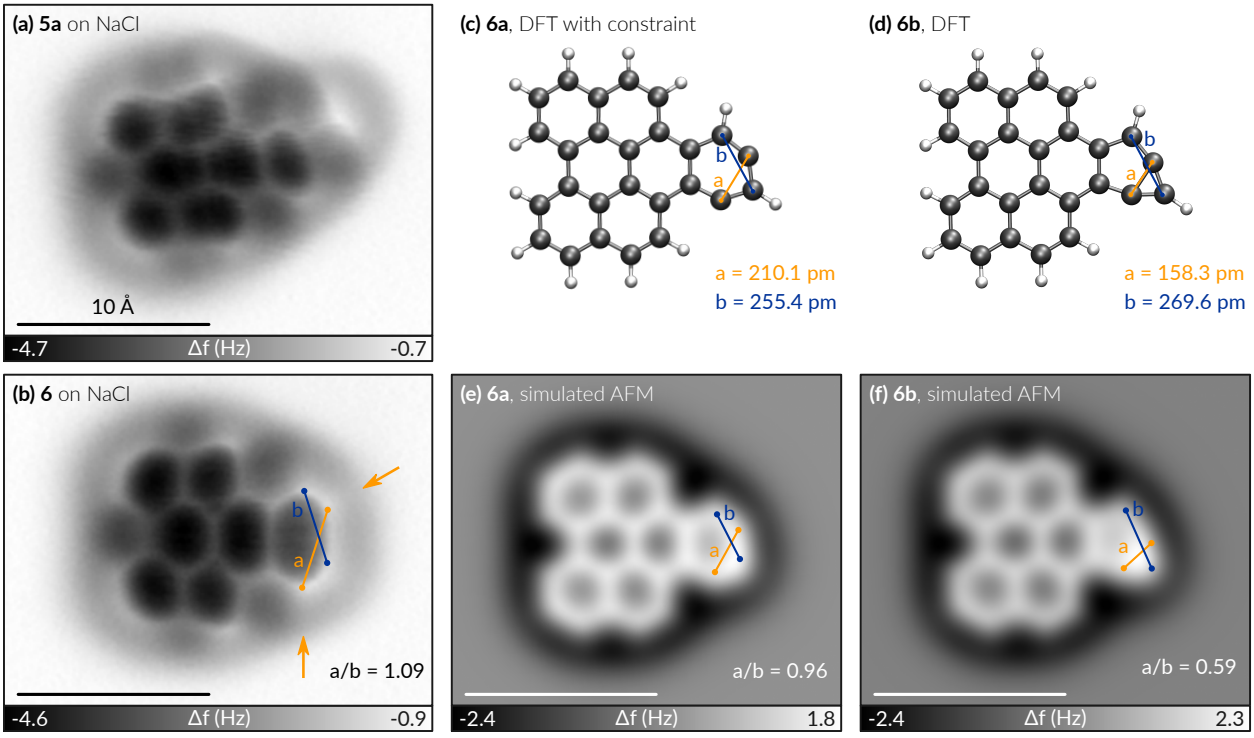

Figure 4: Characterization of *meta*-aryne **6** on NaCl. (a) AFM image of a **5a** molecule ($\Delta z = 152\,\mathrm{pm}$, $I_{\mathrm{sp}} = 1\,\mathrm{pA}$, $V_{\mathrm{sp}} = 0.1\,\mathrm{V}$). (b) AFM image of **6** after atomic manipulation of the molecule **5a** shown in panel a ($\Delta z = 164\,\mathrm{pm}$, $I_{\mathrm{sp}} = 1\,\mathrm{pA}$, $V_{\mathrm{sp}} = 0.1\,\mathrm{V}$). Radical positions are indicated by orange arrows. (c,d) DFT-calculated ball-and-stick models of **6a** and **6b**, respectively. (e,f) Simulated AFM images of **6a** and **6b**, respectively. Distances a (b) are indicated in light orange (dark blue) in panels (b-f). Fig. S3 repeats data of panels (b), (e), and (f) without markup.

enough resolution to distinguish between diradical (**6a**) or anti-Bredt olefin (**6b**) structures. Fig. 4a shows an AFM image of intermediate **5a** on NaCl after the dissociation of the Br-C9 bond by a prior manipulation event on a molecule close-by (see above). The faint lines presumably stem from small movements of the molecule due to interaction with the tip.[32] Next, Fig. 4b shows an AFM image of the *meta*-aryne **6** after a subsequent manipulation event to dissociate the remaining Br atom (the detached Br atom was picked up with the tip at $V = 0$ as reported in Ref. 29, and then a Cu tip was recovered by controlled contact with the Cu surface). STM and scanning tunneling spectroscopy data show that **6** is neutral on this surface[35] as detailed in the Supporting Information (Figure S6). The radical positions of aryne **6** were *a priori* known from the reactant allowing us to analyze the AFM data in Fig. 4b with respect to characteristic features of the radical positions. To this end we have measured the ratio $\frac{a}{b}$ for several individually generated *meta*-arynes, where a and b are the apparent distances between *meta* carbon radicals (marked orange in Fig. 4b) and corresponding saturated carbons (blue), respectively. In spite of errors involved in defining the apparent atomic positions by eye, the measurements are reproducible for different CO tips on different molecules with $1.09 \leq \frac{a}{b} \leq 1.20$. This asymmetry is a distinct feature of *meta*-aryne **6** in contrast to the *ortho*-aryne, 10,11-didehydronaphtho[1,2,3,4-*ghi*]perylene, and the corresponding arene, naphtho[1,2,3,4-*ghi*]perylene, that both appear symmetric.[4] We emphasize that $\frac{a}{b}$ is a ratio of *apparent* distances strongly influenced by tilting of the CO at the tip apex. For example, it has been shown for individual 1,5,9-trioxo-13-aza-triangulene molecules that the same structure can appear qualitatively different with a Xe tip as compared to a CO tip due to electrostatic interactions.[40,41] Nevertheless, the tilting amplifies structural differences in a monotonic way[25,42] as has been demonstrated for a partially fluorinated hydrocarbon.[43] This assumption facilitates to discuss our AFM data pertaining to the controversial reports whether *meta*-arynes adopt a diradical structure **3a** or a bicyclic structure **3b**.[19,22,23] Intuitively, Fig. 4b strongly suggests a diradical structure **6a**. For a well-grounded discussion we additionally simulated AFM images for both possible

structures, **6a** and **6b** (Fig. 4c, Fig. 4d; see Supporting Information), that are displayed in Figs. 4e and 4f, respectively. For the simulated data of the diradical structure, we have used a C9-C11 distance of 210.1 pm as calculated by Sander *et al.*[19] Most importantly, comparison of experimental and simulated AFM data confirms the diradical structure. Beyond that, a is measured longer than b experimentally (Fig. 4b), but $\frac{a}{b} = 0.96$ in the simulation of the diradical structure (Fig. 4e). That is, our data hints to a longer C9-C11 distance for this *meta*-aryne as compared to the *meta*-benzyne in Ref. 19. However, this finding could also be caused by relaxations due to adsorption on the surface, or the tilting of the CO could differ for radical as compared to saturated carbons.

Conclusions

In conclusion, we have demonstrated an on-surface generation procedure of a *meta*-aryne by atomic manipulation of brominated precursor molecules adsorbed on bilayer NaCl islands. On Cu(111) the threshold voltage was significantly larger compared to NaCl, indicating different dissociation mechanisms and the *meta*-aryne product was strongly chemisorbed on the Cu(111) surface. By analyzing the asymmetry of the six-membered ring with the aryne moiety in high-resolution AFM images of the *meta*-aryne adsorbed on NaCl, we have shown a reproducible way to identify the radical positions. Moreover, the AFM data reveals a diradical structure rather than an anti-Bredt olefin structure. It should be mentioned that this is not only a fundamental issue which helps to clarify some past controversial reports. Most of all, this finding could be useful to design on-surface transformations based on meta-aryne intermediates.

Methods

Experimental setup

The experiments were carried out in a homebuilt combined STM and AFM system operated under ultrahigh vacuum conditions (base pressure $p < 10^{-10}$ mbar) at a temperature of $T = 5$ K. Two different qPlus sensors[44,45] (eigenfrequencies $f_0 \approx 26.0$ kHz and 28.8 kHz, respectively; stiffness $k \approx 1.8$ kN/m; quality factor $Q \sim 10^5$) were operated in frequency-modulation mode.[46] The oscillation amplitude was set to $A = 50$ pm. The voltage V was applied to the sample.

STM images were recorded in constant-current mode (closed feedback loop) with a metal-terminated tip and show the topography z. AFM images were acquired with a CO-terminated tip in constant-height mode (open feedback loop) and show the frequency shift Δf. The height offset, Δz, is given for each AFM image with respect to an indicated STM set point above the bare surface (Cu or NaCl). Positive height offsets Δz refer to a distance increase.

Sample preparation

Cu(111) single crystals were cleaned by sputtering and annealing cycles. Experiments were performed on the bare Cu(111) surface, and on islands of two-monolayer thick NaCl. NaCl islands were grown by sublimation from a crucible onto the cleaned Cu(111) surface held at a temperature of $T = 270$ K.[47] Low sub-monolayer coverages of compound **4** and CO molecules were deposited at sample temperatures $T < 10$ K.

Data processing

STM and AFM images, as well as numerically obtained dI/dV curves, were post-processed using Gaussian low-pass filters (full-width at half-maximum corresponds to 1-2 pixels for raw data and 4-6 pixels for Laplace-filtered data of 160×160 to 320×320 pixels).

Apparent distances a and b between *meta* carbon radicals (marked orange in Fig. 4b of the main text) and corresponding saturated carbons (blue) were measured by eye such that their endpoints coincide with vertices of the hexagon.

DFT calculations

The total energy, electron density and molecular orbitals of the free (gas phase) precursor **4** and *meta*-aryne **6** were calculated with DFT.[48] A code with numerical atomic orbitals as the basis functions[49] and the Perdew-Burke-Ernzerhof exchange-correlation functional[50] was applied. The Tkatchenko-Scheffler van-der-Waals method[51] was used. Geometry relaxation was performed with the *really tight* basis defaults until atomic forces converged to 10^{-4} eV/Å. To enforce the diradical structure, we constrained the atomic positions of C-9 and C-11 with their distance set to 210.1 pm (taken from CCSD calculations in Ref. 19) and let all other atoms relax.

Simulated AFM images

We have used a numerical method considering the relaxation of a probe particle (corresponding to, in our case, a CO molecule) due to the tip-molecule interaction to simulate AFM images.[42] The model is based on empirical Lennard-Jones potentials. The atomic positions were taken from the DFT-calculated geometries. The lateral stiffness of the CO molecule was set to 0.29 N/m, a value that was determined independently for *ortho*-[4] and *para*-arynes.[5] The simulated AFM images correspond to a nominal distance of 7.8 Å (before relaxation of the probe particle) between the molecular plane and the tip base.

Acknowledgement

We acknowledge S. Fatayer for fruitful discussions and R. Allenspach for comments on the manuscript. The research leading to these results received funding from the ERC Advanced

Grant CEMAS (agreement no. 291194), the ERC Consolidator Grant AMSEL (682144), the EU project PAMS (610446), the Agencia Estatal de Investigación (MAT2016-78293-C6-3-R and CTQ2016-78157-R), the Xunta de Galicia (Centro singular de investigación de Galicia accreditation 2016-2019, ED431G/09) and the European Regional Development Fund (ERDF).

Supporting Information

1. Synthesis and spectroscopic characterization of **4**.

2. Additional STM/AFM data.

References

1. Leung, L.; Lim, T.; Ning, Z.; Polanyi, J. C. Localized Reaction at a Smooth Metal Surface: *p*-Diiodobenzene at Cu(110). *J. Am. Chem. Soc.* **2012**, *134*, 9320–9326.

2. Huang, K.; Leung, L.; Lim, T.; Ning, Z.; Polanyi, J. C. Single-Electron Induces Double-Reaction by Charge Delocalization. *J. Am. Chem. Soc.* **2013**, *135*, 6220–6225.

3. Huang, K.; Leung, L.; Lim, T.; Ning, Z.; Polanyi, J. C. Vibrational Excitation Induces Double Reaction. *ACS Nano* **2014**, *8*, 12468–12475.

4. Pavliček, N.; Schuler, B.; Collazos, S.; Moll, N.; Pérez, D.; Guitián, E.; Meyer, G.; Peña, D.; Gross, L. On-surface Generation and Imaging of Arynes by Atomic Force Microscopy. *Nature Chem.* **2015**, *7*, 623–628.

5. Schuler, B.; Fatayer, S.; Mohn, F.; Pavliček, N.; Moll, N.; Meyer, G.; Peña, D.; Gross, L. Reversible Bergman Cyclization by Atomic Manipulation. *Nature Chem.* **2016**, *8*, 220–224.

6. Anggara, K.; Huang, K.; Leung, L.; Chatterjee, A.; Cheng, F.; Polanyi, J. C. Clocking Surface Reaction by In-Plane Product Rotation. *J. Am. Chem. Soc.* **2016**, *138*, 7377–7385.

7. Anggara, K.; Huang, K.; Leung, L.; Chatterjee, A.; Cheng, F.; Polanyi, J. C. Bond Selectivity in Electron-Induced Reaction Due to Directed Recoil on an Anisotropic Substrate. *Nature Comm.* **2016**, *7*, 13690.

8. Simic Milosevic, V.; Mehlhorn, M.; Morgenstern, K. Imaging the Bonds of Dehalogenated Benzene Radicals on Cu(111) and Au(111). *ChemPhysChem* **2016**, *17*, 2679–2685.

9. Gross, L.; Mohn, F.; Moll, N.; Liljeroth, P.; Meyer, G. The Chemical Structure of a Molecule Resolved by Atomic Force Microscopy. *Science* **2009**, *325*, 1110–1114.

10. de Oteyza, D. G.; Gorman, P.; Chen, Y. C.; Wickenburg, S.; Riss, A.; Mowbray, D. J.; Etkin, G.; Pedramrazi, Z.; Tsai, H.-Z.; Rubio, A. *et al.* Direct Imaging of Covalent Bond Structure in Single-Molecule Chemical Reactions. *Science* **2013**, *340*, 1434–1437.

11. Riss, A.; Paz, A. P.; Wickenburg, S.; Tsai, H.-Z.; de Oteyza, D. G.; Bradley, A. J.; Ugeda, M. M.; Gorman, P.; Jung, H. S.; Crommie, M. F. *et al.* Imaging Single-Molecule Reaction Intermediates Stabilized by Surface Dissipation and Entropy. *Nature Chem.* **2016**, *8*, 678–683.

12. Kawai, S.; Haapasilta, V.; Lindner, B. D.; Tahara, K.; Spijker, P.; Buitendijk, J. A.; Pawlak, R.; Meier, T.; Tobe, Y.; Foster, A. S. *et al.* Thermal Control of Sequential On-Surface Transformation of a Hydrocarbon Molecule on a Copper Surface. *Nature Comm.* **2016**, *7*, 12711.

13. Stetsovych, O.; Švec, M.; Vacek, J.; Chocholoušová, J. V.; Jančařík, A.; Rybáček, J.; Kosmider, K.; Stará, I. G.; Jelínek, P.; Starý, I. From Helical to Planar Chirality by On-Surface Chemistry. *Nature Chem.* **2017**, *9*, 213–218.

14. Kawai, S.; Takahashi, K.; Ito, S.; Pawlak, R.; Meier, T.; Spijker, P.; Canova, F. F.; Tracey, J.; Nozaki, K.; Foster, A. S. *et al.* Competing Annulene and Radialene Structures in a Single Anti-Aromatic Molecule Studied by High-Resolution Atomic Force Microscopy. *ACS Nano* **2017**, *11*, 8122–8130.

15. Marquardt, R.; Sander, W.; Kraka, E. 1,3-Didehydrobenzene (*m*-Benzyne). *Angew. Chem. Int. Ed.* **1996**, *35*, 746–748.

16. Sander, W. *m*-Benzyne and *p*-Benzyne. *Acc. Chem. Res.* **1999**, *32*, 669–676.

17. Kraka, E.; Anglada, J.; Hjerpe, A.; Filatov, M.; Cremer, D. m-Benzyne and Bicyclo[3.1.0]hexatriene – Which Isomer is More Stable? – a Quantum Chemical Investigation. *Chem. Phys. Lett.* **2001**, *348*, 115–125.

18. Winkler, M.; Sander, W. The Structure of *meta*-Benzyne Revisited: A Close Look into σ-Bond Formation. *J. Phys. Chem. A* **2001**, *105*, 10422–10432.

19. Sander, W.; Exner, M.; Winkler, M.; Balster, A.; Hjerpe, A.; Kraka, E.; Cremer, D. Vibrational Spectrum of *m*-Benzyne: A Matrix Isolation and Computational Study. *J. Am. Chem. Soc.* **2002**, *124*, 13072–13079.

20. Wenk, H. H.; Winkler, M.; Sander, W. One Century of Aryne Chemistry. *Angew. Chem. Int. Ed.* **2003**, *42*, 502–528.

21. Al-Saidi, W. A.; Umrigar, C. J. Fixed-node Diffusion Monte Carlo Study of the Structures of *m*-Benzyne. *J. Chem. Phys.* **2008**, *128*, 154324.

22. Hess Jr., B. A. Do Bicyclic Forms of *m*- and *p*-Benzyne Exist? *Eur. J. Org. Chem.* **2001**, *2001*, 2185–2189.

23. Hess Jr., B. A. On the Structure of *m*-Benzynes. *Chem. Phys. Lett.* **2002**, *352*, 75–78.

24. de Oteyza, D. G.; Pérez Paz, A.; Chen, Y.-C.; Pedramrazi, Z.; Riss, A.; Wickenburg, S.; Tsai, H.-Z.; Fischer, F. R.; Crommie, M. F.; Rubio, A. Noncovalent Dimerization after Enediyne Cyclization on Au(111). *J. Am. Chem. Soc.* **2016**, *138*, 10963–10967.

25. Gross, L.; Mohn, F.; Moll, N.; Criado, A.; Schuler, B.; Criado, A.; Guitián, E.; Peña, D.; Gourdon, A.; Meyer, G. Bond-Order Discrimination by Atomic Force Microscopy. *Science* **2012**, *337*, 1326–1329.

26. Pavliček, N.; Fleury, B.; Neu, M.; Niedenführ, J.; Herranz-Lancho, C.; Ruben, M.; Repp, J. Atomic Force Microscopy Reveals Bistable Configurations of Dibenzo[*a,h*]thianthrene and their Interconversion Pathway. *Phys. Rev. Lett.* **2012**, *108*, 086101.

27. Schuler, B.; Liu, W.; Tkatchenko, A.; Moll, N.; Meyer, G.; Mistry, A.; Fox, D. J.; Gross, L. Adsorption Geometry Determination of Single Molecules by Atomic Force Microscopy. *Phys. Rev. Lett.* **2013**, *111*, 106103.

28. Hla, S.-W.; Bartels, L.; Meyer, G.; Rieder, K.-H. Inducing All Steps of a Chemical Reaction with the Scanning Tunneling Microscope Tip: Towards Single Molecule Engineering. *Phys. Rev. Lett.* **2000**, *85*, 2777–2780.

29. Mohn, F.; Schuler, B.; Gross, L.; Meyer, G. Different Tips for High-Resolution Atomic Force Microscopy and Scanning Tunneling Microscopy of Single Molecules. *Appl. Phys. Lett.* **2013**, *102*, 073109.

30. Majzik, Z.; Cuenca, A. B.; Pavliček, N.; Miralles, N.; Meyer, G.; Gross, L.; Fernández, E. Synthesis of a Naphthodiazaborinine and Its Verification by Planarization with Atomic Force Microscopy. *ACS Nano* **2016**, *10*, 5340–5345.

31. Pavliček, N.; Gross, L. Generation, Manipulation and Characterization of Molecules by Atomic Force Microscopy. *Nat. Rev. Chem.* **2017**, *1*, 0005.

32. Pavliček, N.; Mistry, A.; Majzik, Z.; Moll, N.; Meyer, G.; Fox, D. J.; Gross, L. Synthesis and Characterization of Triangulene. *Nature Nanotech.* **2017**, *12*, 308–311.

33. Blanksby, S. J.; Ellison, G. B. Bond Dissociation Energies of Organic Molecules. *Acc. Chem. Res.* **2003**, *36*, 255–263.

34. Kawai, S.; Foster, A. S.; Canova, F. F.; Onodera, H.; Kitamura, S.-i.; Meyer, E. Atom Manipulation on an Insulating Surface at Room Temperature. *Nature Comm.* **2014**, *5*, 4403.

35. Repp, J.; Meyer, G.; Olsson, F. E.; Persson, M. Controlling the Charge State of Individual Gold Adatoms. *Science* **2004**, *305*, 493–495.

36. Schendel, V.; Borca, B.; Pentegov, I.; Michnowicz, T.; Kraft, U.; Klauk, H.; Wahl, P.; Schlickum, U.; Kern, K. Remotely Controlled Isomer Selective Molecular Switching. *Nano Lett.* **2015**, *16*, 93–97.

37. Ladenthin, J. N.; Grill, L.; Gawinkowski, S.; Liu, S.; Waluk, J.; Kumagai, T. Hot Carrier-Induced Tautomerization within a Single Porphycene Molecule on Cu(111). *ACS Nano* **2015**, *9*, 7287–7295.

38. Steurer, W.; Fatayer, S.; Gross, L.; Meyer, G. Probe-Based Measurement of Lateral Single-Electron Transfer Between Individual Molecules. *Nature Comm.* **2015**, *6*, 8353.

39. van der Lit, J.; Boneschanscher, M. P.; Vanmaekelbergh, D.; Ijäs, M.; Uppstu, A.; Ervasti, M. M.; Harju, A.; Liljeroth, P.; Swart, I. Suppression of Electron–Vibron Coupling in Graphene Nanoribbons Contacted *via* a Single Atom. *Nature Comm.* **2013**, *4*, 2023.

40. Hapala, P.; Švec, M.; Stetsovych, O.; van der Heijden, N. J.; Ondráček, M.; van der Lit, J.; Mutombo, P.; Swart, I.; Jelínek, P. Mapping the Electrostatic Force Field of Single Molecules from High-Resolution Scanning Probe Images. *Nature Comm.* **2016**, *7*, 11560.

41. van der Heijden, N. J.; Hapala, P.; Rombouts, J. A.; van der Lit, J.; Smith, D.; Mutombo, P.; Švec, M.; Jelínek, P.; Swart, I. Characteristic Contrast in Δf_{min} Maps of Organic Molecules Using Atomic Force Microscopy. *ACS Nano* **2016**, *10*, 8517–8525.

42. Hapala, P.; Kichin, G.; Wagner, C.; Tautz, F. S.; Temirov, R.; Jelínek, P. Mechanism of High-Resolution STM/AFM Imaging with Functionalized Tips. *Phys. Rev. B* **2014**, *90*, 085421.

43. Moll, N.; Schuler, B.; Kawai, S.; Xu, F.; Peng, L.; Orita, A.; Otera, J.; Curioni, A.; Neu, M.; Repp, J. *et al.* Image Distortions of a Partially Fluorinated Hydrocarbon Molecule in Atomic Force Microscopy with Carbon Monoxide Terminated Tips. *Nano Lett.* **2014**, *14*, 6127–6131.

44. Giessibl, F. J. High-speed Force Sensor for Force Microscopy and Profilometry Utilizing a Quartz Tuning Fork. *Appl. Phys. Lett.* **1998**, *73*, 3956.

45. Giessibl, F. J. Advances in Atomic Force Microscopy. *Rev. Mod. Phys.* **2003**, *75*, 949–983.

46. Albrecht, T. R.; Grütter, P.; Horne, D.; Rugar, D. Frequency Modulation Detection Using High-Q Cantilevers for Enhanced Force Microscope Sensitivity. *J. Appl. Phys.* **1991**, *69*, 668.

47. Bennewitz, R.; Barwich, V.; Bammerlin, M.; Loppacher, C.; Guggisberg, M.; Baratoff, A.; Meyer, E.; Meyer, E.; Güntherodt, H. J. Ultrathin Films of NaCl on Cu(111): A LEED and Dynamic Force Microscopy Study. *Surf. Sci.* **1999**, *438*, 289–296.

48. Hohenberg, P.; Kohn, W. Inhomogeneous Electron Gas. *Phys. Rev.* **1964**, *136*, B864–B871.

49. Blum, V.; Gehrke, R.; Hanke, F.; Havu, P.; Havu, V.; Ren, X.; Reuter, K.; Scheffler, M. *Ab Initio* Molecular Simulations with Numeric Atom-Centered Orbitals. *Computer Physics Communications* **2009**, *180*, 2175–2196.

50. Perdew, J. P.; Burke, K.; Ernzerhof, M. Generalized Gradient Approximation Made Simple. *Phys. Rev. Lett.* **1996**, *77*, 3865–3868.

51. Tkatchenko, A.; Scheffler, M. Accurate Molecular Van Der Waals Interactions from Ground-State Electron Density and Free-Atom Reference Data. *Phys. Rev. Lett.* **2009**, *102*, 073005.

Graphical TOC Entry

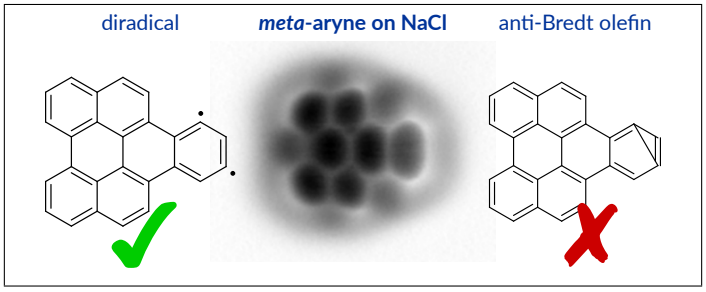

Generation and Characterization of a *meta*-Aryne on Cu and NaCl Surfaces

Supporting Information

Niko Pavliček, Zsolt Majzik, Sara Collazos, Gerhard Meyer, Dolores Pérez, Enrique Guitián, Diego Peña, and Leo Gross

E-mail:

Contents

S1 Synthesis and spectroscopic characterization of 4

S1.1 General methods

All reactions were carried out under argon using oven-dried glassware. TLC was performed on Merck silica gel 60 F254; chromatograms were visualized with UV light (254 and 360 nm). Flash column chromatography was performed on Merck silica gel 60 (ASTM 230 – 400 mesh). ^{1}H NMR spectra were recorded at 300 and 125 MHz (Bruker Varian Mercury-300 instrument), respectively. Low-resolution electron impact mass spectra were determined at 70 eV on a HP-5988A instrument. High-resolution mass spectra (HRMS) were obtained on a Micromass Autospec spectrometer. UV/Vis spectra were obtained on a Varian Cary 100 Bio or a Jasco V-530 spectrophotometers. Fluorescence spectra were obtained on a Fluoromax-2 spectrometer.

Triflate **7** (Scheme S1), precursor of the aryne 3,5-dibromobenzyne (**8**), was prepared following a published procedure.[1,2] *n*-BuLi was used in solution in hexane (2.5 M). Commercial reagents and anhydrous solvents were purchased from ABCR GmbH or Aldrich Chemical Co., and were used without further purification.

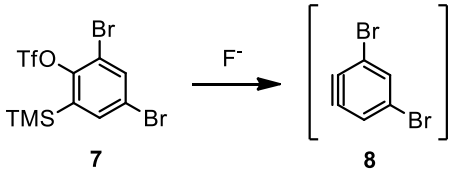

Scheme S1: Fluoride-induced generation of aryne **8** from triflate **7**.

S1.2 Experimental details and spectroscopic data

Dibromonaphthoperylene **4** was prepared by reaction of perylene (**9**) with triflate **7**, which generates aryne **8** in the presence of fluoride (Scheme S2). This synthetic protocol is based on the Diels-Alder reaction between the perylene bay region and an aryne, a reaction that has been previously employed by our group in the synthesis of several naphthoperylene

derivatives in good yields.[3,4] By contrast, compound **4** was isolated in low yields, probably due to the poor efficiency on the fluoride-induced generation of aryne **8** from triflate **7** (Scheme S1), which competes with a thia-Fries rearrangement as it has been reported.[2]

S1.2.1 Synthesis of 9,10-dibromonaphtho[1,2,3,4-*ghi*]perylene (4)

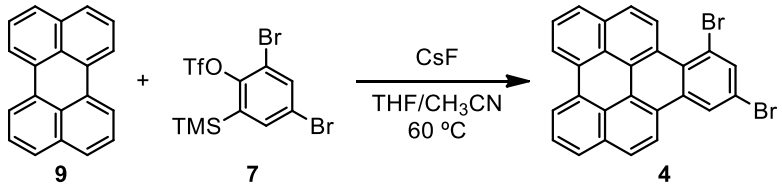

Scheme S2: Synthesis of naphthoperylene **4**.

A mixture of perylene (**9**, 50 mg, 0.198 mmol), triflate **7** (360 mg, 0.794 mmol) and CsF (362 mg, 2.38 mmol) in THF/CH_3CN (1:1, 8 mL) was stirred at 60 °C. After 16 h, the residue was purified by column chromatography (SiO_2; 10% CH_2Cl_2 in hexane) to obtain compound **4** (6.8 mg, 7%) as an orange solid. ^{1}H NMR (298 K, 300 MHz, $CDCl_3$), δ: 9.82 (d, J = 9.3 Hz, 1H), 9.10 (s, 1H), 8.84 (d, J = 7.7 Hz, 2H), 8.70 (d, J = 9.3 Hz, 1H), 8.31 (s, 1H), 8.17 – 8.07 (m, 4H), 7.94 (d, J = 7.2 Hz, 2H) ppm. MS (EI), m/z (%): 484 (90), 404 (7) 324 (100). HRMS (EI) for $C_{26}H_{12}Br_2$, calculated: 483.9285, found: 483.9278.

S1.3 UV/Vis and fluorescence spectra of compound 4

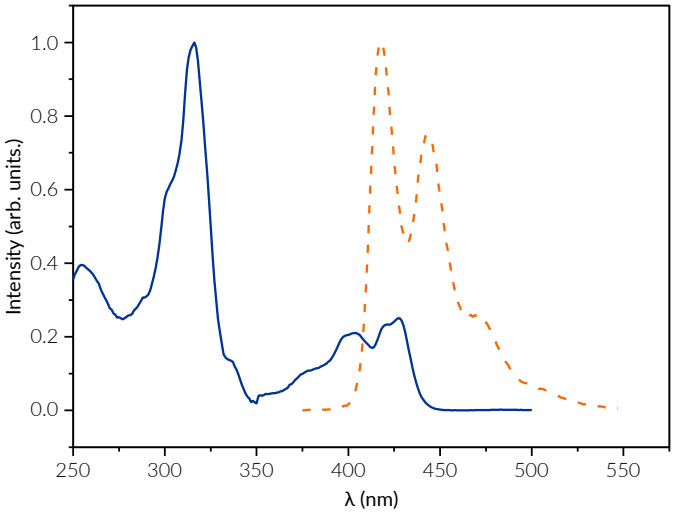

Figure S1: Absorption (solid blue line) and emission (dashed orange line) spectra of compound **4** in CH_2Cl_2.

S1.4 ^{1}H NMR spectrum of compound 4

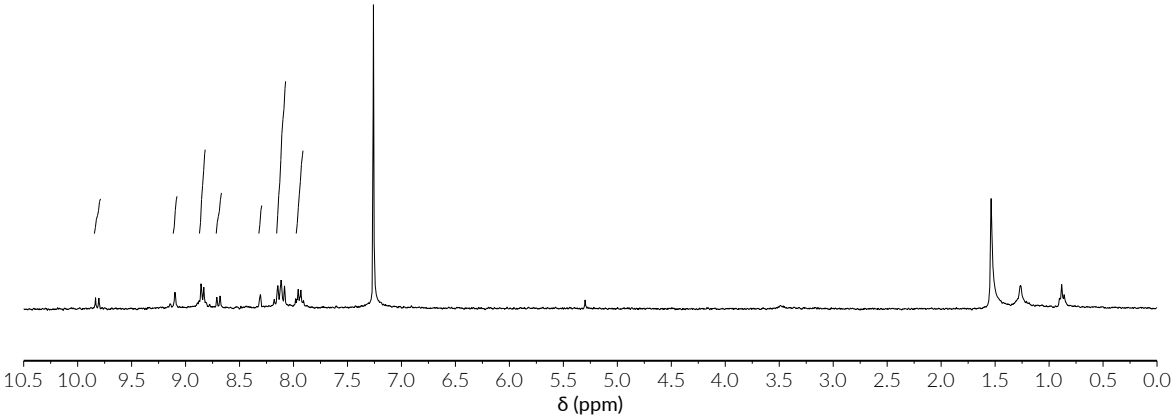

Figure S2: ^{1}H NMR spectrum of compound **4** in $CDCl_3$.

S2 Additional STM/AFM data

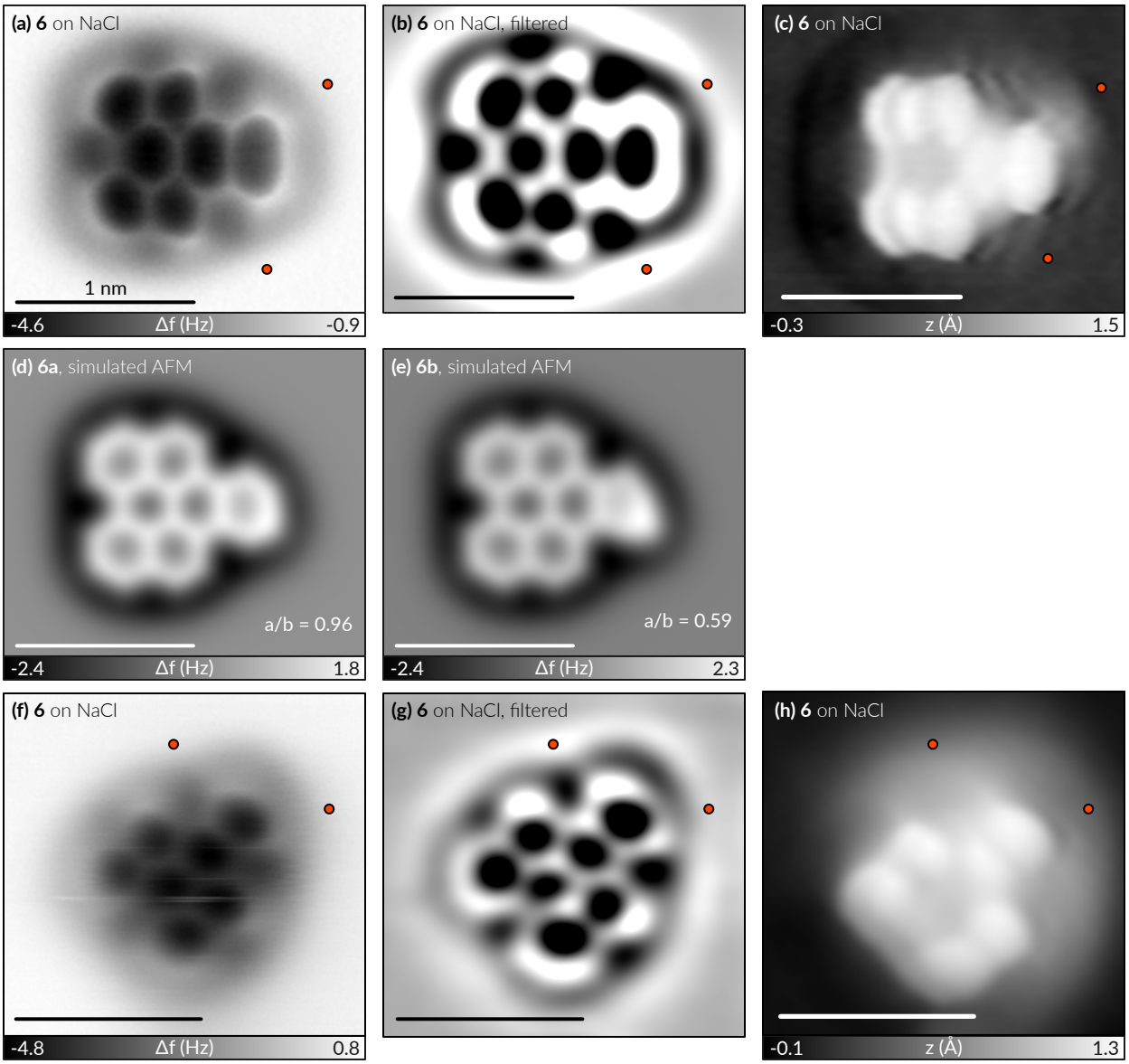

Figure S3: Data from Fig. 4 without overlays (a) AFM image of **6** shown in Fig. 4(a) of the main text. (b) Laplace-filtered version of (a). (c) Corresponding STM image (CO tip). (d) Simulated AFM image of **6a** shown in Fig. 4(e) of the main text. (e) Simulated AFM image of **6b** shown in Fig. 4(f) of the main text. (f,g) Another example of an AFM image of **6** and its Laplace-filtered version, respectively. (h) Corresponding STM image (CO tip). Red dots indicate radical positions.

The data of Fig. 4 of the main text is repeated in Fig. S3a without the overlays indicating lengths a and b. In addition, a Laplace-filtered version of the AFM image is shown in Fig. S3b

to highlight the vague asymmetry indicating the radical positions. Simulated AFM images of **6a** and **6b** are shown in Fig. S3c and S3d, respectively.

An additional example of a *meta*-aryne **6** on NaCl is shown in Fig. S3f. This AFM image was recorded with increased number of pixels (640 px instead of 320 px per line). This facilitates identification of the radical positions by the faint dip in the attractive background because of the missing H atom.

In both cases, corresponding STM images (Fig. S3c and Fig. S3h) show distinct features at each of the radical positions. This observation is another proof that the molecules have not been passivated by atomic hydrogen.

S2.1 Alternative adsorption geometry of 4 on NaCl

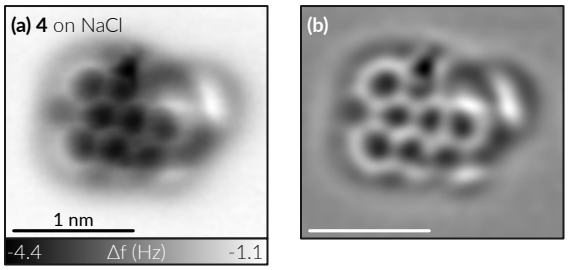

Figure S4: Alternative adsorption geometry of **4** on NaCl. (a) AFM image of **4** (Δz = 170 pm, $I_{sp} = 1$ pA, $V_{sp} = 0.1$ V). (b) Laplace-filtered version of (a).

We have also found precursor molecules **4** adsorbed differently on NaCl as compared to Fig. 1d,e. This alternative geometry is shown in Fig. S4. Strong distortions in the polycyclic backbone are visible because this geometry is less stable and the molecule rotates frequently between two orientations. However, the Br connected to C-9 appears with a different contrast as compared to Fig. 1d,e suggesting different adsorption heights. The initial adsorption geometry of **4** on NaCl had no influence on the on-surface generation of *meta*-aryne **6**.

S2.2 Alternative adsorption geometry of 6 on Cu

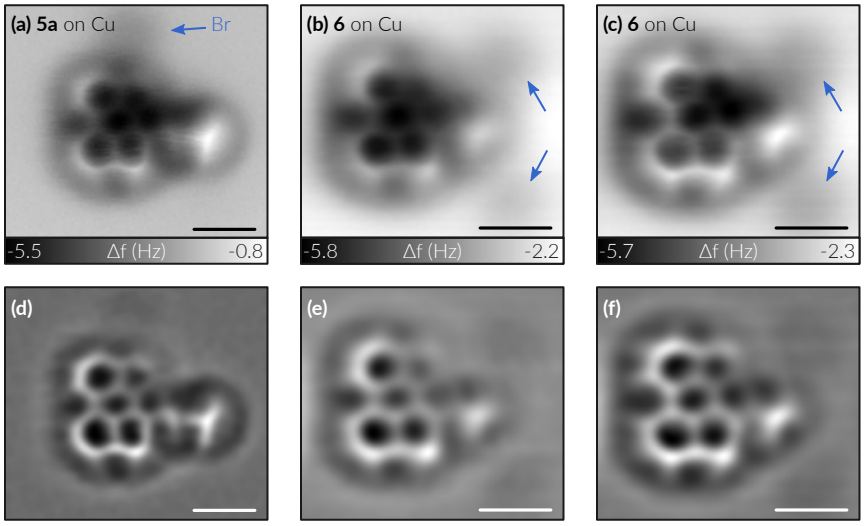

Figure S5: Additional debromination sequence of **4** on Cu(111). (a) AFM image of **5a** ($\Delta z = -120\,\mathrm{pm}$, $I_{sp} = 1\,\mathrm{pA}$, $V_{sp} = 0.1\,\mathrm{V}$). (b,c) AFM images of **6** at far ($\Delta z = -150\,\mathrm{pm}$, $I_{sp} = 0.5\,\mathrm{pA}$, $V_{sp} = 0.1\,\mathrm{V}$) and close ($\Delta z = -183\,\mathrm{pm}$) distance, respectively. (d-f) Laplace-filtered versions of (a-c), respectively. Cleaved Br atoms are indicated by blue arrows in the AFM images.

Presumably depending on the adsorption site, aryne **6** can also adopt different adsorption geometries as demonstrated by another instance of AFM images in Figs. S5a,b. This finding can be rationalized by different reaction pathways. For example, the reaction intermediate **5a**, shown in Fig. S5c, adopts a tilted adsorption geometry hinting to a covalent bond at its radical position C-9. This indicates that, if the Br are detached one-at-a-time, the intermediate **5a** is bound to a certain position. An ensuing manipulation step will detach the second Br from C-11, but the product cannot overcome the reaction barrier to adopt a lower energy adsorption geometry.

S2.3 Charge-state determination of 6 adsorbed on NaCl

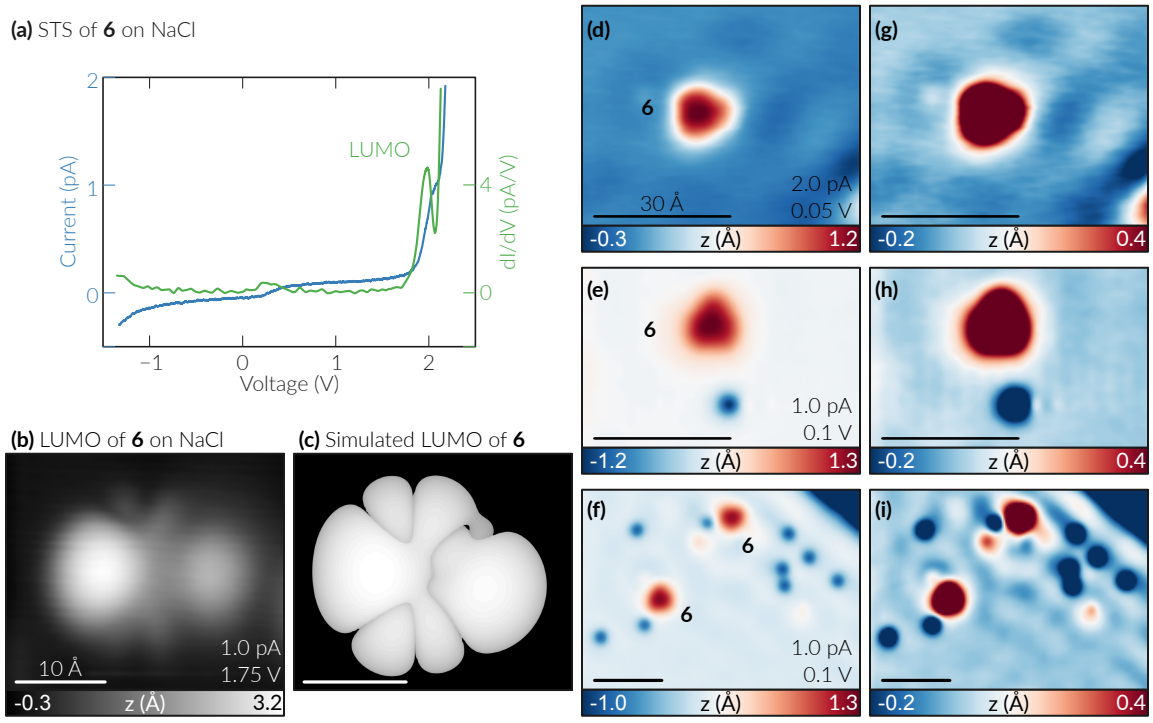

Figure S6: Electronic characterization of **6** on NaCl. (a) STS data of **6** recorded above the center of a molecule. (b,c) Experimental and simulated STM images associated with tunneling into the LUMO of **6**, respectively. (d-f) Three examples of STM images of **6** molecules recorded at low voltages, which are shown additionally with enhanced contrast in panels (g-i). Imaging parameters are given in each panel.

Fig. S6a shows a scanning tunneling spectrum (STS) of an aryne **6** on NaCl. There is a single peak associated with tunneling into the LUMO of the molecule. A corresponding STM image (Fig. S6b) qualitatively agrees with simulated STM data (Fig. S6c). The simulated STM image was calculated as the overlap integral of the molecular orbital and an extended *s*-like wave function for the tip.[5] The absence of any circular scattering patterns centered around the molecules in Figs. S6d-i is an additional proof of their neutral charge state.[6,7] In contrast, the two Br ions in Fig. S6i clearly scatter the interface state electrons.

References

(1) Peña, D.; Cobas, A.; Pérez, D.; Guitián, E. *Synthesis* **2002**, *2002*, 1454–1458.

(2) Hall, C.; Henderson, J. L.; Ernouf, G.; Greaney, M. F. *Chem. Commun.* **2013**, *49*, 7602–7604.

(3) Schuler, B.; Collazos, S.; Gross, L.; Meyer, G.; Pérez, D.; Guitián, E.; Peña, D. *Angewandte Chemie International Edition* **2014**, *53*, 9004–9006.

(4) Pavliček, N.; Schuler, B.; Collazos, S.; Moll, N.; Pérez, D.; Guitián, E.; Meyer, G.; Peña, D.; Gross, L. *Nature Chem.* **2015**, *7*, 623–628.

(5) Pavliček, N.; Repp, J.; Swart, I.; Meyer, G.; Niedenführ, J. *Phys. Rev. Lett.* **2013**, *110*, 136101.

(6) Repp, J.; Meyer, G.; Olsson, F. E.; Persson, M. *Science* **2004**, *305*, 493–495.

(7) Swart, I.; Sonnleitner, T.; Repp, J. *Nano Lett.* **2011**, *11*, 1580–1584.